TABLE II
CODING RESULTS. TOTAL BITS AND RATES REQUIRED FOR THE EXPERIMENT TEXTURES (RIGHT COLUMN GIVES REQUIRED JPEG RATE)

Texture Number	*Indeterministic Components*	*Deterministic Components*	*Total (Including 8-bits for Mean)*	*Number of Bits/Pixel*	
				Model Based Coding	*JPEG*
1	74	480	554	0.14	1.16
2	74	592	666	0.16	1.28
3	90	520	610	0.15	1.56
4	60	864	924	0.23	1.24
5	202	136	338	0.08	0.76
6	267	584	851	0.21	1.36

We present in Figs. 2 and 3 the original, the model-based reconstruction, and the JPEG reconstruction for the six textures at the coding rates given in Table II. Despite the higher rates, the JPEG reconstructions are inferior to the model-based ones, as they display blocking effects and tend to smooth the characteristic roughness of the textures. It is evident that our coding method obtains a high-quality rendition of the original and is superior to the JPEG method applied at much higher rates.

V. CONCLUSIONS

We have presented a novel approach for coding textured images whereby the images are decomposed into a 2-D Wold-like representation, and the parameters of this representation are encoded. We have proved, through enactment of a coding scheme for the parameters, that both high-quality reconstructions and low bit rates are simultaneously achievable for a wide variety of natural textures. We conclude that this new approach is promising and viable for encoding of textured images.

REFERENCES

[1] J. M. Francos, A. Z. Meiri, and B. Porat, "A unified texture model based on a 2-D Wold like decomposition," *IEEE Trans. Signal Processing*, vol. 41, pp. 2665–2678, Aug. 1993.

[2] ——, "A Wold-like decomposition of 2-D discrete homogeneous random fields," *Annals Appl. Prob.*, vol. 5, pp. 248–260, Feb. 1995.

[3] M. Kunt, A. Ikonomopoulos, and M. Kocher, "Second generation image coding techniques," *Proc. IEEE*, vol. 73, pp. 549–574, Apr. 1985.

[4] B. Friedlander, "Lattice filters for adaptive processing," *Proc. IEEE*, vol. 70, pp. 829–867, Aug. 1982.

[5] W. A. Pearlman and R. M. Gray, "Source coding of the discrete Fourier transform," *IEEE Trans. Inform. Theory*, vol. IT-24, pp. 683–692, Nov. 1978.

[6] J. M. Francos, A. Narasimhan, and J. W. Woods, "Maximum likelihood parameter estimation of textures using a Wold decomposition based model," *IEEE Trans. Image Processing*, vol. 4, pp. 1655–1666, Dec. 1995.

Model-Based Reconstruction of Multiple Circular and Elliptical Objects from a Limited Number of Projections

S. Wang, B. Liu, and S. R. Kulkarni

***Abstract*—We consider tomographic image reconstruction from a limited number of noisy projections. An efficient algorithm based on maximum likelihood estimation (MLE) is developed to reconstruct images of multiple discs with unknown locations and radii. The algorithm is successfully applied to images with signal-to-noise ratio (SNR) as low as 0 dB, using as few as 16 projections, and containing as many as twelve discs with widely varying radii. Experimental results show that our approach significantly outperforms conventional convolution back projection. The algorithm is successfully extended to the multiple ellipse case.**

I. INTRODUCTION

The Radon transform of a two-dimensional (2-D) image

$$g(\theta,t)=\int_{-\infty}^{\infty}\int_{-\infty}^{\infty} f(x,y)\delta(t-x\sin\theta-y\cos\theta)\,dx\,dy \qquad (1)$$

maps the image $f(x,y)$ into another 2-D function $g(\theta,t)$. Various techniques for inverting $g(\theta,t)$ lay the ground for reconstruction of a 2-D image from integral projections. It is well known that when the projections are limited in number or view angle, or have high noise levels, it is generally not possible to reconstruct the image accurately using conventional approaches such as filtered back projection. It is reasonable to expect that with prior information about the image, such as a parametrized model of the image, better quality of the reconstruction is achievable. Rossi and Willsky [1] investigated the case of reconstruction of an image of a single disc with known radius and uniform intensity on a known background by estimating the location of the disc using maximum likelihood estimation (MLE). Rossi *et al.* [3] proposed an algorithm for reconstructing an elliptical object using a maximum likelihood (ML) method. Milanfar [4] used ML to reconstruct a binary polygonal image. In his study, moments of the polygon were estimated from the projection data, and then were used to generate an initial guess for the ML algorithm. When there is more than one disc, the computational complexity of MLE grows exponentially. Thus, the approach is impractical even for a moderate image size and more than one disc. Sauer and Liu [2] developed an algorithm for the detection and estimation of multiple discs of equal and known radius with complexity similar to that of the single disc case, and performance very close to that of MLE.

In this paper, we extend the Sauer-Liu algorithm of [2] to the case of multiple discs with unknown radii. We are able to detect the number of discs and estimate both locations and radii of the discs with computational complexity that is linear in the number of discs and the number of possible locations and radii for each disc. The algorithm is further extended to the case in which the image contains multiple ellipses.

Manuscript received August 6, 1995; revised February 5, 1996. This work was supported by a grant from Siemens Corporation. The associate editor coordinating the review of this manuscript and approving it for publication was Prof. Andrew E. Yagle.

The authors are with the Department of Electrical Engineering, Princeton University, Princeton, NJ 08544 USA (e-mail: kulkarni@ee.princeton.edu).

Publisher Item Identifier S 1057-7149(96)05266-9.

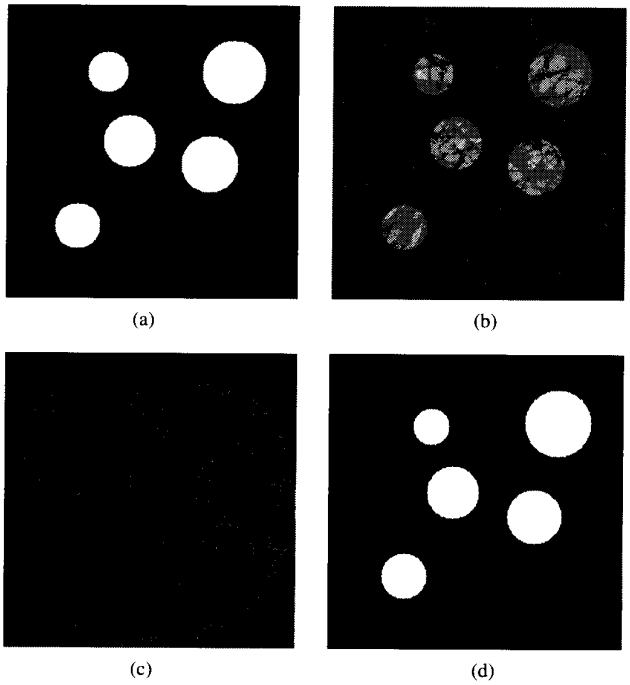

Fig. 1. (a) Original image of five discs. (b) Reconstructed image using CBP and 16 projections when no noise is added. (c) Reconstructed image using CBP and 16 projections when SNR = 10 dB. (d) Reconstructed image using MLE and 16 projections when SNR = 10 dB.

II. Maximum Likelihood Estimation of Parameters

A. Circular Discs

We model the image $f(x,y)$ as the superposition of N discs. Thus

$$f(x,y) = \sum_{i=1}^{N} f_i(x,y;x_i,y_i,r_i) \tag{2}$$

where each f_i has known constant intensity in a disc with center at (x_i,y_i) and radius r_i and is zero elsewhere, i.e.,

$$f_i(x,y) = \begin{cases} 1 & (x-x_i)^2+(y-y_i)^2 \le r_i^2 \\ 0 & (x-x_i)^2+(y-y_i)^2 > r_i^2. \end{cases} \tag{3}$$

The number N, the locations, and the radii are unknown. Let $g_i(\theta,t;x_i,y_i,r_i)$ denote the Radon transform of $f_i(x,y;x_i,y_i,r_i)$. Let $\hat{g}(\theta,t)$ be the noisy observation. Then $\hat{g}(\theta,t) = g(\theta,t)+n(\theta,t)$ where $g(\theta,t)$ is the Radon transform of $f(x,y)$, and $n(\theta,t)$ denotes the noise that is assumed to be independent identically distributed (i.i.d.) Gaussian with zero mean and variance σ^2. The log-likelihood function for the N-disc field can be written as

$$\begin{aligned} L_N(\hat{g},\Omega) &= -\int_0^{\pi}\int_{-\infty}^{\infty}\Big(\hat{g}(\theta,t)-\sum_{i=1}^{N} g_i(\theta,t;x_i,y_i,r_i)\Big)^2\,dt\,d\theta \\ &= -\int_0^{\pi}\int_{-\infty}^{\infty}\hat{g}^2(\theta,t)\,dt\,d\theta + 2\sum_{i=1}^{N}\int_0^{\pi}\int_{-\infty}^{\infty}\hat{g}(\theta,t) \\ &\quad \cdot g_i(\theta,t;x_i,y_i,r_i)\,dt\,d\theta \\ &\quad -\sum_{i=1}^{N}\sum_{j=1}^{N}\int_0^{\pi}\int_{-\infty}^{\infty} g_i(\theta,t;x_i,y_i,r_i) \\ &\quad \cdot g_j(\theta,t;x_j,y_j,r_j)\,dt\,d\theta \end{aligned} \tag{4}$$

where Ω is the parameter set $[x_1,y_1,r_1,x_2,y_2,r_2,\cdots,x_N,y_N,r_N]$ and g_i is the Radon transform of f_i. The first term on the right side of (4) is independent of Ω and can be ignored in the computing of the MLE. By regrouping the second and the third term and dropping the first term, we can rewrite (4) as

$$\tilde{L}_N(\hat{g},\Omega) = 2\sum_{i=1}^{N}\Psi_i - \sum_{i=1}^{N}\sum_{j=1,j\ne i}^{N}\Phi_{ij} \tag{5}$$

where

$$\begin{aligned} \Psi_i &= \int_0^{\pi}\int_{-\infty}^{\infty}\hat{g}(\theta,t)g_i(\theta,t;x_i,y_i,r_i)\,dt\,d\theta \\ &\quad -\tfrac{1}{2}\int_0^{\pi}\int_{-\infty}^{\infty} g_i^2(\theta,t;x_i,y_i,r_i)\,dt\,d\theta \end{aligned} \tag{6}$$

and

$$\Phi_{ij} = \int_0^{\pi}\int_{-\infty}^{\infty} g_i(\theta,t;x_i,y_i,r_i)g_j(\theta,t;x_j,y_j,r_j)\,dt\,d\theta. \tag{7}$$

The square term is included in Ψ_i so that Ψ_i contains all terms depending on a single g_i, while Φ_{ij} accounts for all the cross-terms. The Φ_{ij} can be precomputed, the evaluation of the likelihood function is simple for any given parameter set Ω, but the search for the MLE has complexity $O((MR)^N)$, where M is the number of possible locations for the centers of the discs and R is the number of possible values for the radii of the discs. Thus direct optimization of (4) is impractical even for a few discs. Note that when the projections are taken from limited angles, the only change in the log-likelihood function is that the integral over θ is taken over a subset $S \subset [0,\pi]$ rather than over the whole $[0,\pi]$ range.

B. Ellipses

For the case of multiple ellipses, the image can be modeled as

$$f(x,y) = \sum_{i=1}^{N} f_i(x,y;x_i,y_i,a_i,b_i,o_i) \tag{8}$$

where each f_i has known constant intensity in an ellipse centered at (x_i,y_i) with a_i and b_i being its major and minor axes and o_i being its orientation, i.e.,

$$f_i(x,y) = \begin{cases} 1 & \dfrac{((x-x_i)\cos o_i+(y-y_i)\sin o_i)^2}{a_i^2} \\ & \quad +\dfrac{((y-y_i)\cos o_i-(x-x_i)\sin o_i)^2}{b_i^2} \\ & \quad \le 1 \\ 0 & \text{otherwise.} \end{cases} \tag{9}$$

With $\hat{g}$ denoting the projection data and g_i the Radon transform of f_i, the log-likelihood function can be written as

$$\begin{aligned} L_N(\hat{g},\Omega) &= -\int_0^{\pi}\int_{-\infty}^{\infty}\Big(\hat{g}(\theta,t) \\ &\quad -\sum_{i=1}^{N} g_i(\theta,t;x_i,y_i,a_i,b_i,o_i)\Big)^2\,dt\,d\theta \\ &= -\int_0^{\pi}\int_{-\infty}^{\infty}\hat{g}^2(\theta,t)\,dt\,d\theta \\ &\quad +2\sum_{i=1}^{N}\int_0^{\pi}\int_{-\infty}^{\infty}\hat{g}(\theta,t) \\ &\quad \cdot g_i(\theta,t;x_i,y_i,a_i,b_i,o_i)\,dt\,d\theta \\ &\quad -\sum_{i=1}^{N}\sum_{j=1}^{N}\int_0^{\pi}\int_{-\infty}^{\infty} g_i(\theta,t;x_i,y_i,a_i,b_i,o_i) \\ &\quad \cdot g_j(\theta,t;x_j,y_j,a_j,b_j,o_j)\,dt\,d\theta. \end{aligned} \tag{10}$$

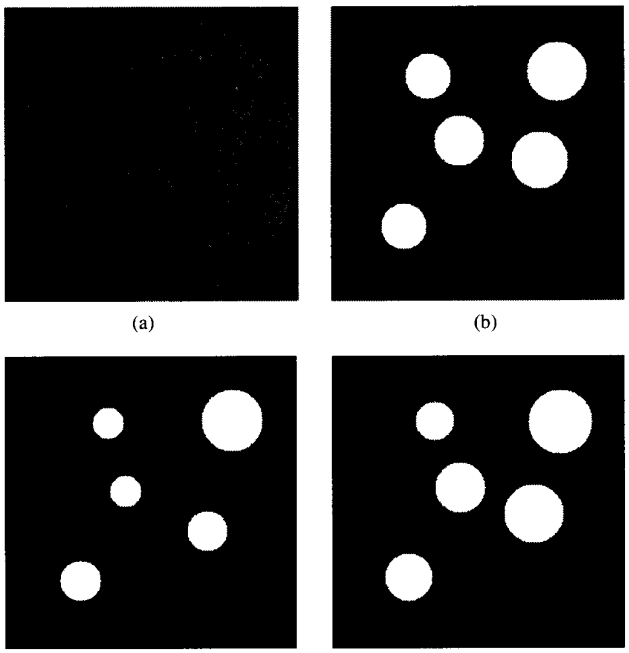

(a) (b) (c) (d)

Fig. 2. (a) Reconstructed image using CBP and 32 projections when SNR = 0 dB. (b) Reconstructed image using MLE and 32 projections when SNR = 0 dB. (c) Reconstructed image using MLE and 16 projections within angles 45° to 135° when SNR = 10 dB. (d) Reconstructed image using MLE and eight projections from angles 45° to 90° and eight projections from 135° to 180° when SNR = 10 dB.

III. Detection and Estimation of Multiple Discs

A. Algorithm

Sauer and Liu [2] proposed an algorithm for the detection and estimation of multiple discs that are of the same known radius. The algorithm has complexity near that of the single disc case, and with performance very close to that of the MLE. We extend this algorithm to the case where the radii are varying and unknown, but take values from a finite set.

First, we divide the possible locations of the center (i.e., the whole image field) into $K \times K$ blocks. Within each block, we find a maximum for Ψ_i as defined in (6), among all possible values of x, y with the block and all possible r, and we retain only those with positive Ψ. After this step, we have a set of candidate locations and radii. Normally, N will be large enough that $\tilde{L}_N(\hat{g}, \Omega)$ will be negative because of the Φ term in (5).

The number of candidate discs is then reduced by iteration. At each step, among the N candidates, we evaluate $\tilde{L}_{N-1}(\hat{g}, \Omega)$ for all combinations of $N-1$ candidates, and retain those $N-1$ candidates with the largest $\tilde{L}_{N-1}$. The iteration stops when further reduction will not increase the likelihood function.

After the pruning of the candidate set, we perturb each remaining candidate over an area at least four times the size of original detection block and over all possible radii. This step resembles the direct global search for the MLE, but with complexity linear in N.

Finally, we scan the whole image field to see if the likelihood function can be increased by adding a new disc. The process stops when adding a new disc will not increase the likelihood function. Perturbation of each of the current discs is done after each addition.

A multiresolution approach is used when the search is through all the possible radii. We divide the possible radii into several subsets and pick one element from each subset. We first search through the representative elements, then search though the subset corresponding to the best representative. In doing so, we reduce the complexity to a fraction of NMR, with M being the number of possible locations and R being the number of possible radii.

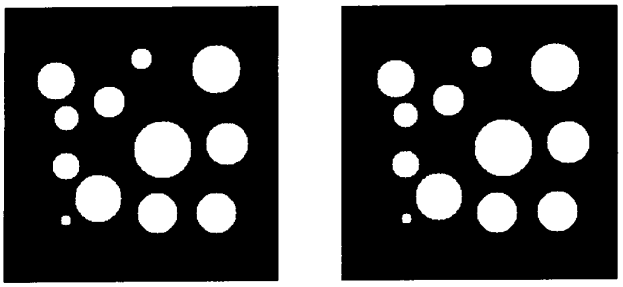

(a) (b)

Fig. 3. (a) Original image of 12 discs. (b) Reconstructed image using MLE and 32 projections when SNR = 20 dB.

B. Experimental Results

We define the SNR in the Radon transform as

$$\text{SNR} = 10 \log \left(\frac{\max_{\theta,t} g^2(\theta, t)}{\sigma^2} \right). \tag{11}$$

Typical experimental cases have as inputs the projections from 16 or 32 equally spaced angles, with each projection sampled at 256 values of t. The radii of the discs in the experimental images are integers between 5 and 35, and the block size constant K equals 16 in our experiments. We compare the reconstructed images using convolution backprojection (CBP) and the approach proposed in this paper, which, for simplicity, shall be referred to as MLE reconstruction.

Fig. 1(a) is the original image with five discs. Fig. 1(b)–(d) shows the reconstructed image with 16 projections using (b) CBP and no noise added, (c) CBP with SNR = 10 dB, and (d) our MLE method with SNR = 10 dB. Fig. 2(a) and (b) show the reconstructed image with 32 projections using a) CBP with SNR = 0 dB and b) our MLE method with SNR = 0 dB. We have also considered cases in which the projections are taken from a limited angle. Fig. 2(c) and (d) shows the reconstructed image using our MLE method when c) 16 projections are taken equally spaced between 45° and 135° with SNR = 10 dB and d) eight projections are taken from angles between 45° and 90° and the other eight projections are taken from angles between 135° and 180°. Fig. 3(a) shows an original image with 12 discs, and Fig. 3(b) is the reconstructed image using our MLE method when 32 projections are used and SNR = 20 dB. At SNR = 10 dB, the MLE reconstruction is about identical to Fig. 3(b) except that the smallest disc is not detected. Most of the positions and radii of the circles were estimated either correctly or to within one pixel. None of the estimated positions were more than four pixels off, and none of the estimated radii were more than two pixels off.

C. Performance Analysis

For performance analysis, both analytical approaches and simulations are difficult for multiple discs due to the large number of parameters. We want performance analysis primarily for qualitative insight, so for simplicity we consider only the case of a single disc. Analysis of estimating the center was considered by Rossi and Willsky in [1]. Hence, we consider a single disc centered at the origin and analyze the performance in estimating r.

We have done simulations both as a function of the radius and as a function of the noise level. Fig. 4(a) shows the mean squared

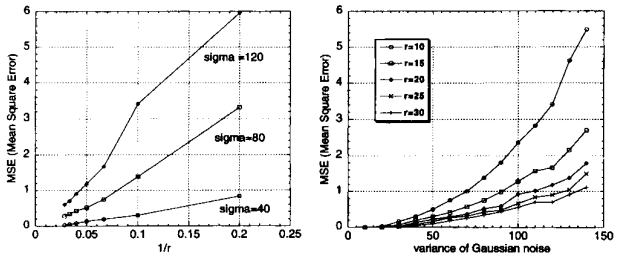

Fig. 4. (a) MSE versus r with single disc located at the origin. (b) MSE versus σ with single disc located at the origin.

error (MSE) as a function of $1/r$ for three values of σ, and Fig. 4(b) shows the MSE as a function of σ for five values of r. Each point in the figures was obtained using 1000 randomly generated noisy projection data sets and computing the resulting MSE. Note that from the figures it appears that the MSE is approximately linear in $1/r$, and the MSE is approximately quadratic in σ, the standard deviation of the Gaussian noise.

We verify the qualitative aspects in the simulation results through an analytical computation. The lack of smoothness and functional form of the image of an ideal disc causes problems with the analysis. Hence, following [3], for analytical tractability, we model the image as $f(x,y) = e^{-(x^2+y^2)/r^2)}$ so that $\hat{g}(\theta,t) = g(\theta,t) + n(\theta,t)$ where

$$g(\theta,t) = \int_{-\infty}^{\infty} e^{-(t^2+y^2)/r^2)}\, dy.$$

The likelihood function can be written as

$$L(r) = \frac{1}{\sigma^2}\int_0^{\pi}\int_{-\infty}^{\infty} \hat{g}(\theta,t)g(\theta,t)\, dt\, d\theta - \frac{1}{2\sigma^2}\int_0^{\pi}\int_{-\infty}^{\infty} g(\theta,t)^2\, dt\, d\theta \tag{12}$$

and the Fisher information is

$$I = -E\frac{\partial^2 L(r)}{\partial r^2} = \frac{\pi}{\sigma^2}\int_{-\infty}^{\infty}\left(\frac{\partial g(\theta,t)}{\partial r}\right)^2 dt = \frac{3\pi^2\sqrt{2\pi}}{8\sigma^2}r. \tag{13}$$

Hence, the Cramer–Rao lower bound on the variance of the estimate is $8\sigma^2/(3\pi^2\sqrt{2\pi}r)$, which qualitatively matches our simulation results in terms of the behavior as a function of r and σ.

IV. Detection and Estimation of Multiple Ellipses

A. Algorithm

For the case of multiple ellipses, we first use the algorithm proposed in the previous section to detect a set of circular discs and obtain an estimate of their locations and radii. Then we set the initial values of the ellipses based on the results we obtain from the first search. For each ellipse, the center will be the center of the disc and the major and minor axes are $r+\delta$ and $r-\delta$, respectively, with the orientation set to be zero and δ a fixed positive constant. In some cases, some of the detected discs overlap one another or are within a small distance d. These discs are then treated as a single disc whose center is the centroid of the centers of those discs and whose radius is such that the single disc covers all the overlapping discs.

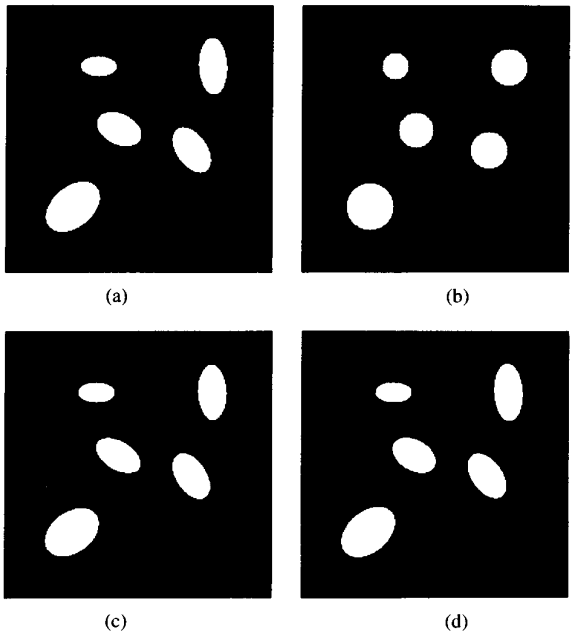

Fig. 5. (a) Original image of five ellipses. (b) Ellipses first are detected as discs when SNR = 15 dB and 32 projections are used. (c) Reconstructed image using MLE when SNR = 15 dB and 32 projections are used. (d) Reconstructed image using MLE when SNR = 30 dB and 16 projections are used.

Now we fix the location of all the ellipses and search through their axes and orientation. For each ellipse, we search through all possible combinations of major and minor axes in the range $(a-\Delta, a+\Delta)$ and $(b-\Delta, b+\Delta)$ and the orientations of every 15 degrees, i.e., $0°, 15°, 30°, \cdots, 165°$, where a and b are the initial values of the major and minor axes. After finding the values of the major axis, minor axis, and orientation that maximize that likelihood function, we go on to search the next ellipse. After searching the last ellipse, we come back to the first one, and the process continues until the likelihood function will not increase after one round of search. This process is repeated and the only difference is that for each ellipse, the searching range of the orientation is between $\theta-7°$ and $\theta+8°$ where θ is the orientation of the ellipse and the searching step size is $1°$.

Next, we fix the major and minor axes and the orientations of the ellipses. Following similar steps as above, we move the center of each ellipse around a neighborhood to find the position that maximizes the likelihood function. Combined with the major and minor axes and the orientation we obtained during the previous step, we now have the final result of estimation.

Suppose N is the number of ellipses, A and B are the numbers of the possible values of major and minor axes, respectively, and Θ is the number of possible orientations. Then the computation complexity for our algorithm is $O(N\Theta AB)$. Note that for a brute force MLE search, the computation complexity is $O((\Theta AB)^N)$.

When two or more ellipses are too close to each other, our algorithm cannot distinguish them from a single ellipse; thus, in this situation our algorithm fails.

B. Experimental Results

In our experiments, we take δ to be 2, Δ to be 5, and d to be 5. Fig. 5(a) is the original image consisting of five ellipses

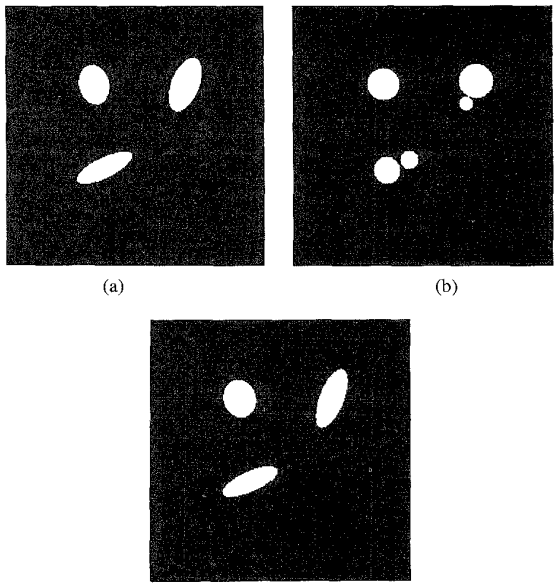

Fig. 6. (a) Original image of three ellipses. (b) Ellipses first are detected as discs when SNR = 15 dB and 32 projections are used. (c) Reconstructed image using MLE when SNR = 15 dB and 32 projections are used.

with eccentricities ranging from 1.5 to 2.0. Fig. 5(b) shows the intermediate results when the ellipses are first detected as discs when SNR = 15 dB and 32 projections are used. Fig. 5(c) is the final reconstruction result using our maximum likelihood method in this case. Fig. 5(d) is the final reconstruction result when SNR = 30 dB and 16 projections are used. Fig. 6(a) is the original image consisting of 3 ellipses with eccentricities of 1.3, 2.0, and 3.0. Fig. 6(b) shows the intermediate results when the ellipses are first detected as discs. Note that there are five discs in the figure. Those discs that are close enough to each other are treated as one single disc. Fig. 6(c) shows the reconstructed result using MLE when SNR = 15 dB and 32 projections are used. The estimated ellipse positions and major and minor axis were either correct or at most one or two pixels off, and the estimated orientations were usually within 2°, and in all cases within 6°.

V. Conclusions

When the SNR is low and the number of projections is small, a model-based MLE approach is an effective method in reconstructing images consisting of discs of unknown locations and radii. The approach is also effective in reconstructing images consisting of multiple ellipses, where the positions, major and minor axes, and orientations are all unknown. For multiple discs or ellipses in the image, a brute force MLE method will have exponential complexity, thus is hardly implementable. We have developed an efficient algorithm to solve this problem, and good experimental results are achieved using our algorithm.

To avoid the "overfitting" problem of detecting an eccentric ellipse as multiple circular discs, an interesting alternative might be to iteratively apply the single object methods of [1] and [3]. Specifically, one could first search for a single object of highest energy, subtract the effect of this object, then search for a second object, etc. This might be interesting to pursue for further work.

References

[1] D. J. Rossi and A. S. Willsky, "Reconstruction from projections based on detection and estimation of objects, pts. I and II: performance analysis and robustness analysis," *IEEE Trans. Acoust., Speech, Signal Processing*, vol. ASSP-32, no. 4, pp. 886–906, Aug. 1984.

[2] K. D. Sauer and B. Liu, "Image reconstruction from a limited number of projections using multiple object detection/estimation," in *Proc. ICASSP '90*, vol. 4, pp. 1861–1864, 1990.

[3] D. J. Rossi, A. S. Willsky, and D. M. Spielman, "Object shape estimation from tomographic measurements—a performance evaluation," *Signal Processing*, vol. 18, pp 63–68, Sept. 1989.

[4] P. Milanfar, W. C. Carl, A. S. Willsky, and G. C. Verghese, "Moment-based geometric image reconstruction", in *Proc. ICIP '94*, vol II, pp. 825–829, 1994.

Correction to "Hybrid Poisson/Polynomial Objective Functions for Tomographic Image Reconstruction from Transmission Scans"

Jeffrey A. Fessler

In the above paper,[1] Fig. 7 was repeated and misnamed Fig. 8. The correct Fig. 8 appears below.

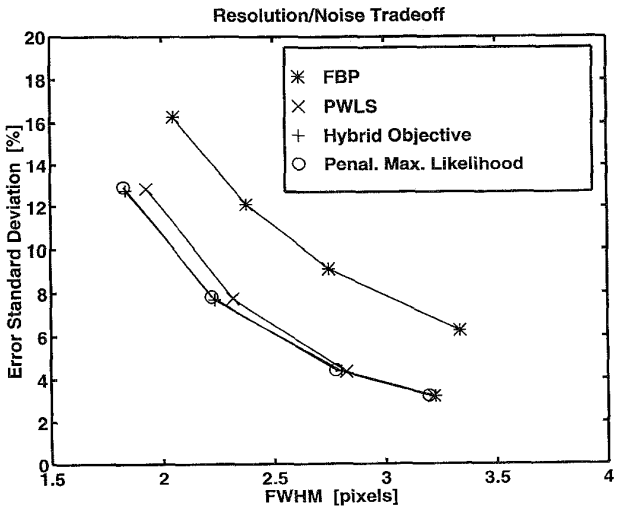

Fig. 8. Resolution versus noise for the various reconstruction algorithms. The FBP method has significantly greater noise than the statistical methods. For finer resolutions, the PWLS estimates are slightly noisier than the PML estimates. The performance of the hybrid objective with $\gamma_a = 5$ and $\gamma_b = 50$ is indistinguishable from penalized likelihood.

Manuscript received July 22, 1994.

The author is with the University of Michigan, Ann Arbor, MI 48109–2122 USA.

Publisher Item Identifier S 1057-7149(96)07155-2.

[1] J. A. Fessler, *IEEE Trans. Image Processing*, vol. 4, no. 10, pp. 1439–1450, Oct. 1995.